Hindawi
Advances in Civil Engineering
Volume 2020, Article ID 1308530, 19 pages
https://doi.org/10.1155/2020/1308530

Research Article

Damage Assessment of an SRC Frame-Core Tube Structure under the Action of a Main Aftershock Sequence

Peng Wang[1,2,3] **Qingxuan Shi**[1,2,3] **Feng Wang,**[2] **and Siusiu Guo**[1,2,3]

[1]*State Key Laboratory of Green Building in Western China, Xi'an University of Architecture & Technology, Xi'an 710055, China*
[2]*School of Civil Engineering, Xi'an University of Architecture & Technology, Xi'an 710055, China*
[3]*Key Lab of Structural Engineering and Earthquake Resistance, Ministry of Education (XAUAT), Xi'an 710055, China*

Correspondence should be addressed to Peng Wang; wangpeng@xauat.edu.cn

Received 26 November 2019; Revised 15 February 2020; Accepted 24 February 2020; Published 6 June 2020

Academic Editor: Ahmed Mebarki

Copyright © 2020 Peng Wang et al. This is an open access article distributed under the Creative Commons Attribution License, which permits unrestricted use, distribution, and reproduction in any medium, provided the original work is properly cited.

Historical seismic damage data show that most strong earthquakes are accompanied by multiple intense aftershocks. In general, the time interval between the main shock and the aftershocks is relatively short, and structure repair work is often not completed before the aftershocks occur. For a structure that has suffered damage from the main shock, the aftershock will further aggravate the damage and even cause complete collapse. Based on the incremental dynamic analysis (IDA) method, this paper establishes a probabilistic seismic demand model for the SRC framework-core tube structure and plots the vulnerability curve of a structure under the action of the main aftershock sequence, which occurs following the actions of frequent earthquakes, fortification earthquakes, and rare earthquakes. The structure vulnerability matrix and the vulnerability index are used to evaluate the seismic performance of a structure. This study found that the occurrence of aftershocks leads the structure to a more unfavourable failure state. Taking the vulnerability index as an evaluation parameter, the structural vulnerability index when subjected to an intensity 8 earthquake under the action of the main aftershock is approximately 10% larger than under the action of a single main shock. Meanwhile, the SRC frame-core structure designed according to the current Chinese specifications meets the expected seismic fortification target, even after being acted upon by the main aftershock ground motion sequence.

1. Introduction

Historical seismic damage data show that most strong earthquakes are accompanied by multiple large intensity aftershocks. Under normal circumstances, the time interval between the main shock and the aftershocks is relatively short, and structure repair work is not completed before the aftershocks occur. At this time, for an engineering structure that has suffered damage from the main shock, the aftershock will further damage the structure and even cause it to completely collapse. In recent years, controlling seismic risk and loss has become a research hotspot in the field of seismic engineering. As a core module of seismic risk analysis, vulnerability analysis has important application value for seismic design, reinforcement, and maintenance decisions for structures. The application and research of steel-reinforced concrete (SRC) frame-core tube structures started late, so research on its seismic performance, seismic damage mechanism, and vulnerability is still in the exploration stage.

1.1. Studies of the Structural Response under the Action of the Main Aftershock. The influence of aftershocks on seismic analysis of structural engineering was first considered by Mahin [1], based on the sequence-type ground motion of two aftershocks. The results show that the energy accumulation and ductility of the structure caused by aftershocks are greatly improved. Amadio et al. [2] studied the response of inelastic single-degree-of-freedom (SDOF) systems under the action of main aftershock ground motion sequence. The results show that system damage increases significantly after the aftershock occurs. Hatzigeorgiou and Beskos [3] and Hatzigeorgiou [4, 5] established a nonlinear SDOF system model considering the effects of postyield stiffness reduction, strength reduction, damping ratio, etc. The inelastic

displacement ratio spectrum of an SDOF system under the main aftershock sequence ground motion was obtained. Furthermore, the ductility demand and displacement coefficient spectrums were obtained in the same way. Zhai et al. [6, 7] proposed a Park–Ang damage spectrum considering the additional structure damage caused by aftershocks based on the study of Hatzigeorgiou et al. [3–5]. Through shaking table experiments, the influence of the main shock/main shock-aftershock on seismic behaviour of reinforced concrete (RC) columns was studied by Twigden et al. [8]. The results show that the aftershocks have a significant influence on the residual displacement of RC columns. Goda and Salami [9] analysed the nonlinear response of a wood frame structure under the main aftershock ground motion sequence using the IDA method. The results show that the structural damage index following an aftershock can increase by 5~20%. Ludovico et al. [10] carried out research on the failure mechanism of damaged RC columns under the action of the main aftershocks and found that the relationship between the yield and residual displacement ratios of the column is roughly parabolic. The damage of the frame-filled wall structure under the action of the main aftershock sequence ground motion was studied by Zhu [11]. The results show that the structure damage increases gradually from top to bottom under the action of the main aftershock, and the plastic hinge distribution and crack development in the structure are quite different from those under the action of the main shock. Hou [12] studied the response of 60 SDOF systems using the main aftershock sequence ground motion. The results show that when the aftershock intensity is larger than that of the main shock, the aftershock has a significant impact on the equal-damage and equal-ductility strength reduction. Tao [13] and Yu et al. [14] studied the incremental damage of the elastoplastic SDOF model with 533 main aftershock sequence ground motions. The results show that medium and long-period structures are more sensitive to aftershocks, and the damage is more serious. The condition of unfavourable main aftershock sequence ground motion is that the predominant period T_M of the main shock is close to the predominant period T_A of the aftershock or T_M is smaller than T_A.

1.2. Research on Structural Seismic Vulnerability. Structural seismic vulnerability refers to the probability of exceeding multiple damage states for a structure under various seismic intensities. In the early period, most of the vulnerability analyses were conducted on nuclear power plants. Hwang and Low [15] took the lead in introducing the idea of seismic vulnerability to building structures and first studied the vulnerability of flat and RC structures. Rossetto and Elnashai [16] conducted a finite element numerical analysis of a structure using the static push-over method and assessed its vulnerability by studying the performance points between the structural demand and response spectrums. Li and Ellingwood [17] studied the effects of various construction methods of main aftershock sequence ground motion on the vulnerability of steel frame structures. The results show that the interstorey drift of the structure is sensitive to the spectral characteristics of the aftershock. Using the IDA method, Ryu et al. [18] analysed the vulnerability curve for the equivalent SDOF system being in a severe damage state, and a calculation method for the vulnerability of damaged structures under earthquake action is also given. Polese et al. [19] studied structure vulnerability under the action of main aftershocks and found that when a structure has moderate or slight damage, the aftershock has little effect on the displacement response, but the ductility requirement of the structure decreases by as much as 40%. Zhang et al. [20] studied the influence of the moment amplifying coefficient of the column end on the vulnerability of RC frame structures. The results show that the structure collapse probability increases with the decreasing bending moment amplifying coefficient. The authors [21–23] conducted a series of studies on the vulnerability of RC frame structures under the action of the main aftershock sequence. The results show that the probability of exceeding the structure damage state under the main aftershock sequence will increase significantly, especially for strong aftershock intensity, and the effect of aftershocks can be effectively reduced by adding steel support to the frame structure. The structural vulnerability index concept was proposed by Yu et al. [24] by combining the damage state probability with the empirical value of the seismic damage index. The index can be used to evaluate the damage degree of RC frame structures when subjected to various intensity ground motions. In addition, some scholars have also studied the vulnerability of super-high-rise mixed structures, chimney structures, and steel grid-concrete frame structures of railway stations [25–28].

From the above previous studies, it is easily determined that there are few studies on structural damage under the action of the main aftershock and additional damage caused by the aftershocks. Additionally, there are few research studies on the vulnerability analysis of the frame-core tube structure. Therefore, it is necessary to make a clear damage assessment by vulnerability analysis of the SRC frame-core tube structure under the main aftershock of the ground motion sequence.

In this paper, a 20-story SRC frame-core tube structure is designed according to the current Chinese code [29]. The finite element model is built by Perform-3D software. Fifteen typical main aftershock ground motions and 15 single main shock ground motions are applied to the structure in the time history analysis. Then, the IDA method is used to establish the probabilistic seismic demand model, and the vulnerability of the SRC frame-core tube structure under the main aftershock sequence ground motion is studied. Finally, the vulnerability matrix of intensity 8 frequent earthquakes, fortification earthquakes, and rare earthquakes is calculated, and the probability of the structure being in various damage states under the frequent, design, and rare earthquakes is analysed. According to the seismic damage index given in the specification [30], the damage status of the SRC frame-core tube structure is evaluated under the main aftershock of the ground motion sequence.

2. Model of the SRC Framework-Core Tube Structure

2.1. Component Model

2.1.1. Model of the Column and Beam. The plastic hinge and fibre models are the two most commonly used analytical models for nonlinear simulated beams and columns. A diagram of the plastic hinge and fibre models is shown in Figure 1. Furthermore, the fibre model accurately simulates the nonlinear behaviour of beams and columns. The fibre model method divides the member into several segments in the longitudinal direction. The deformation of a section in the middle of each segment represents the segment deformation. The force state of the fibre unit is only in one dimension. The strain of the fibre is determined according to the flat section assumption, the generalized stiffness relationship between the internal force and the deformation of the section is obtained by integrating each subblock or layer along the section, and then the stiffness matrix of components is obtained. The beam fibre is distributed in one dimension along the beam depth, whereas the column fibre distribution is in the form of a grid. The length of the SRC beam and column plastic zone is calculated by the method proposed by Bai et al. [31]. The equation is as follows:

$$l_{\mathrm{p}} = \frac{M_{\max} - M_y}{M_{\max}} \times Z, \tag{1}$$

where l_{p} is the length of the plastic zone, $M_{\max}$ and M_y are the ultimate and yielding bending moments of the section, respectively, and Z is the distance from the member end to the antibending point when the section reaches the ultimate bending moment.

2.1.2. Model of the Shear Wall. Models commonly used in Perform-3D to simulate shear walls are the shear and the general wall models. In this paper, the shear wall model is used to simulate the seismic performance of the shear wall. The fibre model is used to simulate the bending moment-axial force (PM) behaviour of the shear wall in plane, and nonlinear shear material is added to simulate horizontal shear failure behaviour. The shear wall model is shown in Figure 2. Moreover, the states of bending, shearing, and torsion resistance of the shear wall outside the plane are considered elastic.

2.1.3. Model of the Coupling Beam. The coupling beam element adopts the ordinary beam element. The bending-axial force (*PM*) performance of the plastic zone at both ends of the coupling beam is simulated by the fibre model, and the shearing hinge is set in the beam element to simulate the shear behaviour of the coupling beam. In addition, the joints of the shear wall element in Perform-3D do not have in-plane rotational stiffness. Therefore, when the coupling beam is connected to the shear wall element, it is necessary to provide an embedded beam with strong bending rigidity to the shear wall element to achieve a rigid connection between the coupling beam and the shear wall, as shown in Figure 3. The bending stiffness of the embedded beam is approximately 20 times the coupling beam, whereas the axial and torsional stiffness are set to small values. This process can be achieved by setting the axial cross-sectional area of the beam element.

2.2. Constitutive Relationship of the Material

2.2.1. Constitutive Model of the Concrete. In elastoplastic time-history analysis, the concrete tensile strength is not considered. The uniaxial concrete compressive stress-strain curve is determined according to the relevant Chinese Code [32] and depicted in Figure 4, where $f_{\mathrm{c,r}}$ is the average value of concrete compressive strength, $\varepsilon_{\mathrm{c,r}}$ is the compressive strain corresponding to the uniaxial compressive strength $f_{\mathrm{c,r}}$, and $\varepsilon_{\mathrm{cu}}$ is the concrete ultimate compressive strain. The Mander model [33] is used to simulate the behaviour of the confined concrete, and its compressive stress-strain curve is depicted in Figure 5, where f_{cc} is the compressive strength of the confined concrete, $\varepsilon_{\mathrm{cc}}$ is the compressive strain corresponding to the compressive strength f_{cc}, and $\varepsilon_{\mathrm{cu}}$ is ultimate compressive strain of the confined concrete.

However, the material constitutive specified in the Perform-3D software is composed of a multiline string, as shown in Figure 6. The points *Y, U, L, R*, and *X* are the five key points of the generalized stress-strain (F-D) curve, where *Y* is the yield point, *U* is the ultimate strength point, *L* is the starting point of strength reduction, *R* is the residual strength point, and *X* is the ultimate deformation point.

Before point *Y* is the elastic section of the line. YU is the strengthening section. Compared with the elastic stiffness, the stiffness of the strengthening section is reduced. UL is the platform section, which is the ideal plastic stage. LR is the falling strength section and the strength reaches point *R*. After that, the value remains unchanged. Point *X* is the control point for calculating whether to terminate the simulation. When the deformation reaches this point, the material is considered to lose strength and the calculation stops. To adapt the constitutive model for concrete material in Perform-3D, the uniaxial compression constitutive curve of concrete and the confined concrete constitutive curve determined by the Mander model are fit to a five-fold line model. The equal-area fitting method proposed by Liu et al. [34] is adopted, which means that the area enclosed by the actual constitutive curve is equal to the area enclosed by the fit polygonal line. The fitting process is depicted in Figure 7. The concrete elastic modulus E_{c} is taken as the initial modulus before yield point *Y*, and the stress is linear with strain. Yield point *Y* corresponds to a strength of $0.30\,\mathrm{F_U}$, and $\mathrm{F_U}$ is the maximum compressive strength. A horizontal line from $0.95\,\mathrm{F_U}$ is depicted intersecting the concrete constitutive curve to obtain two points *U* and *L*. Similarly, a horizontal line from $0.50\,\mathrm{F_U}$ is depicted intersecting with the concrete constitutive curve to obtain one auxiliary point. Then, a horizontal line of $0.20\,\mathrm{F_U}$ connects point *L* with the auxiliary point in a straight line to obtain point *R*. The ultimate strain $\mathrm{D_X}$ is 0.01, which is greater than the ultimate compressive strain of general concrete. The small residual

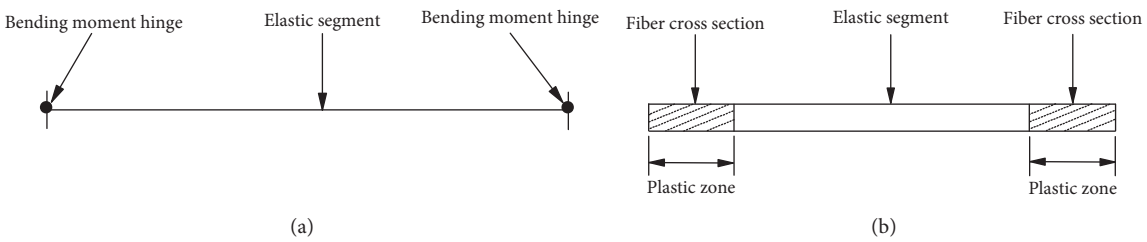

Figure 1: (a) Plastic hinge model. (b) Fibre model.

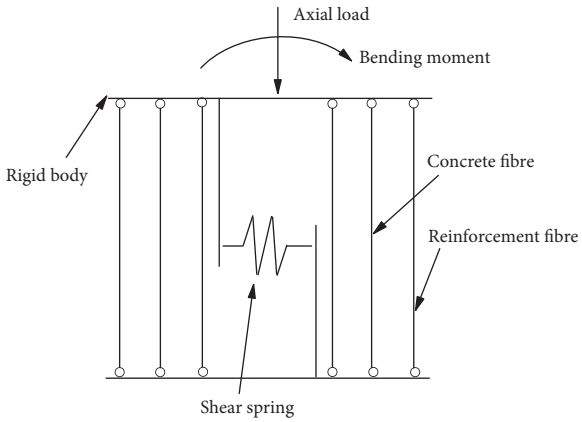

Figure 2: Fibre model of the shear wall.

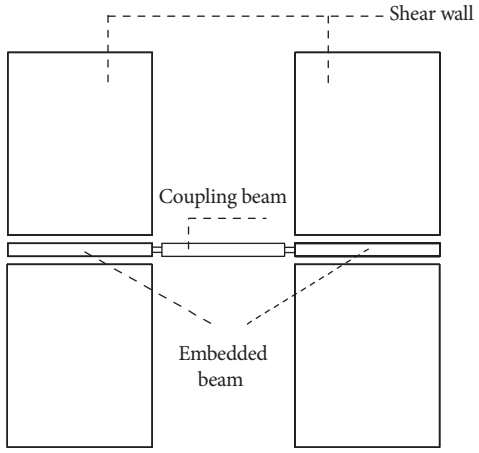

Figure 3: Rigid connection between the coupling beam and the shear wall.

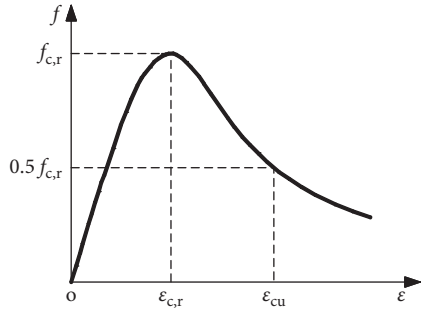

Figure 4: The stress-strain curve of the concrete.

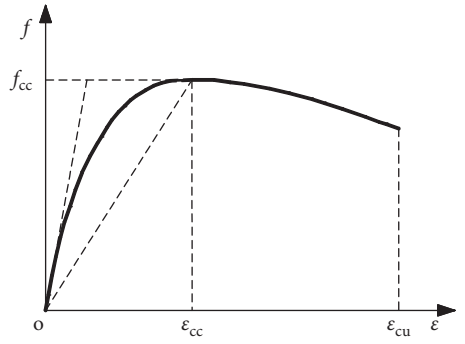

Figure 5: The stress-strain curve of the confined concrete.

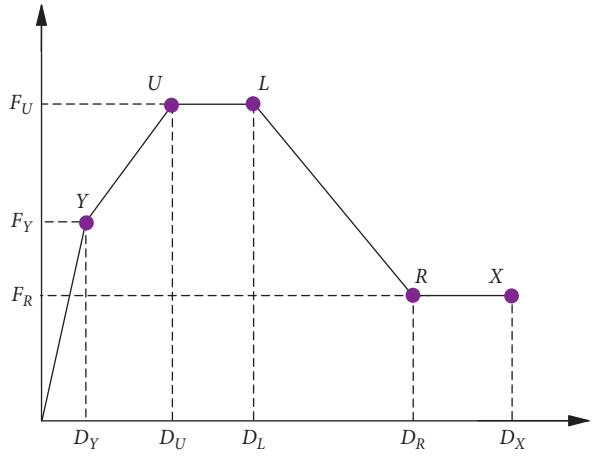

Figure 6: Relationship of F-D in Perform-3D.

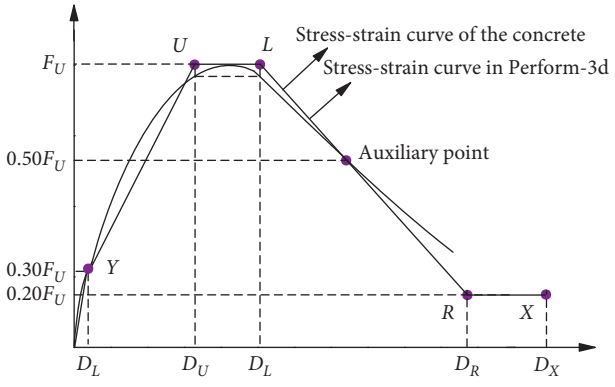

Figure 7: Schematic diagram of concrete material fitting.

strength of the material after reaching the ultimate strain has little effect on the structure; in most cases, before the material strain reaches D_X, the structure has collapsed and the bearing capacity is lost. The concrete material has stiffness degradation under reciprocating seismic loads. Table 1 shows the strength degradation coefficient for each key point of the concrete.

2.2.2. Constitutive Model of the Reinforcing Bar and Steel. According to past engineering experience, the actual working state of steel bars is mostly in the elastic stage. It is also possible to reach the yielding phase under very strong loads, but the probability of entering the strengthening phase is extremely low. Therefore, the steel and reinforcing bars in the structure are simulated using the ideal bilinear elastoplastic model in Perform-3D, as shown in Figure 8, where the ultimate strain D_X is taken as 0.05 as suggested in the FEMA356-06. Similar to concrete, steel bars and steel also exhibit stiffness degradation under earthquake action. Table 1 shows the material degradation coefficients for various key points of steel bars and steel.

2.3. Structural Model Parameters and Dynamic Characteristics Analysis. The structure established and analysed is a steel-reinforced concrete (SRC) frame-reinforced concrete (RC) core tube structure with a total of 20 storeys. Its plane layout is shown in Figure 9, the total height of the structure is 72.6 m, and the height of the first storey is 4.2 m and the other storeys are 3.6 m. The ratio of total height to width is 3.0. The core tube wall thickness of stories 1–10 is 450 mm, and the concrete strength grade of the shear walls and beams and columns is C50; however, the core tube wall thickness from stories 11–20 is 350 mm, and the concrete strength grade of shear walls and beams and columns is C40. The section height of all the coupling beams is 700 mm. The flat slabs 1–10 are made of C40 grade concrete, the flat slabs 11–20 are made of C30 grade concrete, and the floor thickness is 200 mm. The SRC frame-RC core tube structure steel is grade Q345. The longitudinal reinforcement in the walls, beams, and columns is HRB400 grade steel bar, and the hoop reinforcement is HPB300 grade steel bar. The cross-sectional dimension information for each structural component is shown in Table 2. The permanent load of floors 1~19 is 7.5 kN/m^2, the live load of floors 1~2 is 3.5 kN/m^2, the live load of floors 3~19 is 2 kN/m^2, and the dead and live loads of the roof are 9 and 2 kN/m^2, respectively. The structure model established by Perform-3d is shown in Figure 10. The seismic fortification intensity is 8 degrees, the design earthquake group is the second group, the design basic seismic acceleration is 0.2 g, the site category is Class II, the building site characteristic period is 0.40 s, the basic wind pressure is 0.385 kN/m^2, and the site rough type is C. Through simulation analysis, the maximum interlayer drift of the structure under the action of frequent earthquakes is 1/980, which satisfies that the maximum elastic interlayer drift for the frame-core tube structure being less than 1/800 as prescribed by the Chinese code [29].

Table 1: Strength degradation coefficient of materials.

Material	Y	U	L	R	X
Concrete	1	0.9	0.7	0.4	0.3
Steel and steel bars	1	0.55	0.55	0.55	0.55

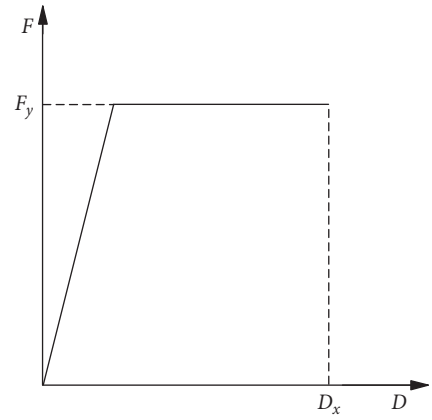

Figure 8: Relationship of F-D for steel and reinforcements.

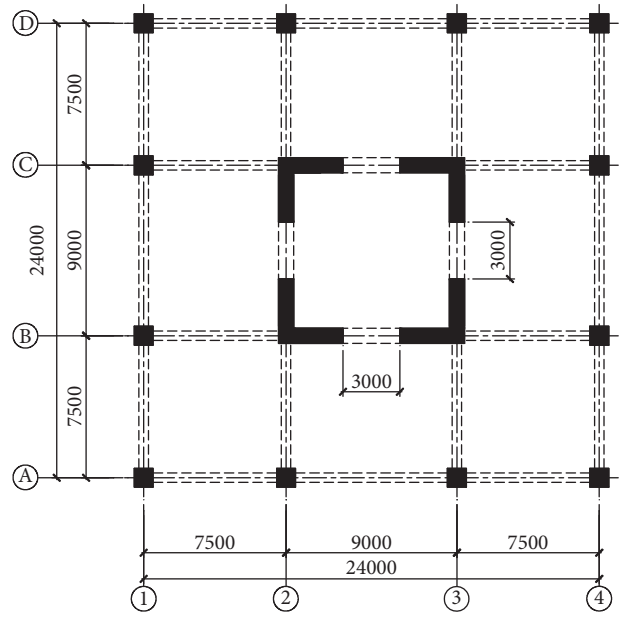

Figure 9: Structure layout.

Modal analysis gives the first 6-order period of the structure, as shown in Table 3, and the first 6-order modes of the structure are shown in Figure 11. It can be seen that the first and second structure mode shapes are both translational, and the third is a rotation shape around the vertical axis. The first-order period is dominated by translation of $T_1 = 1.41$ s, the third-order period is dominated by rotation of $T_t = 1.12$ s, and the ratio of the two periods T_t/T_1 is $= 0.79 < 0.9$, which satisfies the provisions [35]. In addition, by comparison, the first 6-order periods of the structure calculated by Yingjianke and Perform-3D Software are very

Table 2: Section size of the members in the SRC frame-core tube structure.

Members	Cross section		Member arrangement	Section size (mm)	Section size of steel (mm)
Beam	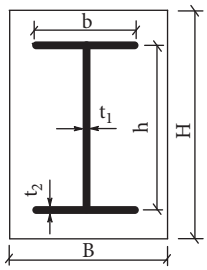	1~10 storeys	Side frame beam	400 × 700	450 × 250 × 20 × 22
			Inner frame beam	350 × 650	400 × 200 × 18 × 20
			Side frame beam	400 × 700	450 × 250 × 20 × 22
		11~20 storeys	Inner frame beam	350 × 650	400 × 200 × 18 × 20
Column	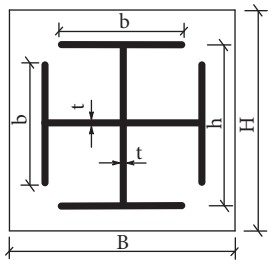	1~10 storeys	Corner column	1000 × 1000	600 × 350 × 25
			Side column	900 × 900	500 × 300 × 22
			Corner column	900 × 900	500 × 300 × 22
		11~20 storeys	Side column	800 × 800	450 × 250 × 18

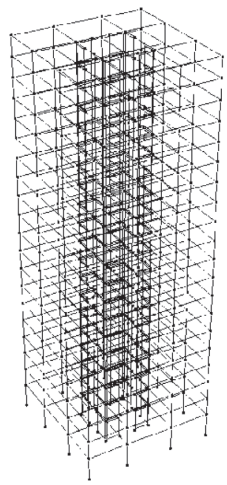

Figure 10: Structure model.

Table 3: The first 6-order period of the structure.

Various software	Orders					
	1	2	3	4	5	6
Yingjianke	1.40	1.40	1.10	0.41	0.40	0.40
Perform-3d	1.41	1.41	1.12	0.41	0.41	0.40

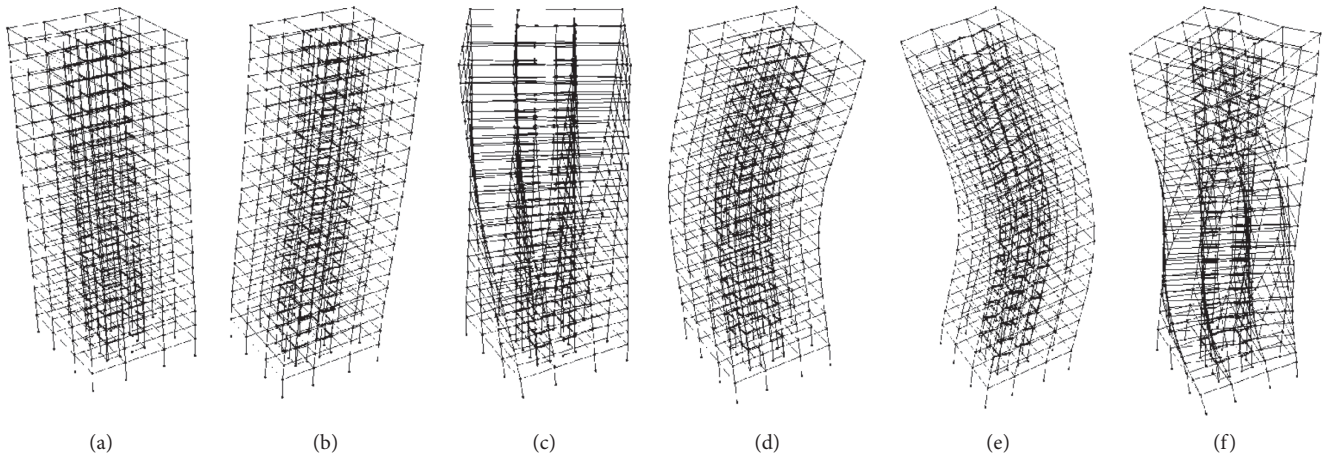

Figure 11: The first 6 modes of the structure. (a) 1st mode. (b) 2nd mode. (c) 3rd mode. (d) 4th mode. (e) 5th mode. (f) 6th mode.

close, which verifies the rationality of the SRC framework-core tube structure model.

3. Ground Motion Sample

In dynamic time-history analysis, the factors affecting structural dynamic response discreteness are as follows: (1) material uncertainty, (2) ground motion uncertainty, (3) geometric size uncertainty, (4) uncertainty of boundary conditions, and (5) uncertainty of model simplification. In structural vulnerability analysis, it is impossible to consider all the factors listed above at the same time, without considerable additional time spent because of the complexity of the random problem. For the research content difference, one kind of uncertainty should reasonably consider the key object of the analysis. Therefore, this paper mainly studies the influence of the main aftershock and aftershock sequence uncertainty on structural vulnerability.

According to the method in Code [29], the ground motion records were selected. In the elastic time-history analysis, the shear force at the bottom of the structure calculated by each ground motion record should not be less than 65% of that calculated by the mode decomposition response spectrum method. The average value of the shear force at the bottom of the structure calculated from multiple ground motion records should not be less than 80% of that calculated by the mode decomposition response spectrum method. The 15 ground motion records finally selected for time-history analysis are shown in Table 4, where T_A is the predominant period of the aftershock and T_M is the predominant period of the main shock.

4. Incremental Dynamic Analysis

4.1. Introduction to the IDA Method. In 1977, Professor Bertero proposed the IDA method. The basic idea draws on the idea of extending single static analysis to incremental in the static push analysis. By extending a single dynamic time-history analysis to an incremental dynamic time-history analysis, the dynamic response of the structure under different input seismic intensities can be obtained. This method is called the incremental dynamic analysis method. When performing IDA analysis, the ground motion intensity measure (IM) and engineering demand parameter (EDP) should be determined in advance. For any increasing ground motion intensity, a relationship curve between the IM and the EDP is established, known as the IDA curve. When multiple ground motions are input to the structure, the IDA curve cluster is obtained. The IDA curve cluster contains two meanings: (1) each IDA curve represents the maximum seismic response of a structure under ground motion; (2) any point on each IDA curve represents the maximum seismic response of the structure under a certain ground motion intensity. By analysing the IDA curve cluster, the structural seismic performance under various seismic intensities can be statistically evaluated.

4.2. Parameter Selection for IDA Analysis

4.2.1. IM. The ground motion intensity index is a parameter that reflects the strength of the ground motion when an earthquake occurs. The commonly used strength indicators are mainly four types: peak acceleration (PGA), peak velocity (PGV), peak displacement (PGD), and acceleration response spectrum S_a (T_1, 5%) based on the first fundamental period of the structure. Studies have shown that the applicable objects and discrete types of each intensity index are quite different in the elastoplastic time-history analysis of structures. The existing research of Zhang [36] shows that for special ground motion such as the main aftershock sequence, the first periodic spectral acceleration intensity index S_a (T_1, 5%) has the highest correlation with structural damage and stability. Then, it effectively reduces the dispersion of the calculation results. Therefore, the index S_a (T_1, 5%) is taken as the control index of the main aftershock sequence ground motion input in this paper.

4.2.2. EDP. The EDP commonly used in structure analyses are base shear force, node rotation angle, structural vertex

Table 4: Information of the main aftershock sequence ground motion.

Station name	Aftershock time	Aftershock magnitude	Main shock (PGA) (g)	Aftershock (PGA) (g)	T_A/T_M
CHY025E	99/09/25	6.30	0.16	0.13	1.50
CHY046N	99/09/20	6.20	0.19	0.11	1.87
CHY047N	99/09/25	6.30	0.18	0.23	1.32
CHY052W	99/09/25	6.30	0.09	0.05	1.69
CHY057E	99/09/20	6.20	0.04	0.02	1.87
CHY063N	99/09/25	6.30	0.07	0.04	1.75
CHY065N	99/09/25	6.30	0.09	0.05	1.31
CHY076E	99/09/20	6.20	0.07	0.04	1.43
CHY080N	99/09/25	6.30	0.86	0.12	1.37
CHY082N	99/09/25	6.30	0.06	0.20	1.63
CHY107W	99/09/20	6.20	0.10	0.04	1.63
HWA002W	99/09/20	6.20	0.05	0.01	1.34
HWA030E	99/09/22	6.20	0.07	0.05	1.53
HWA033E	99/09/20	6.20	0.17	0.02	1.42
HWA035N	99/09/20	6.90	0.07	0.02	1.07

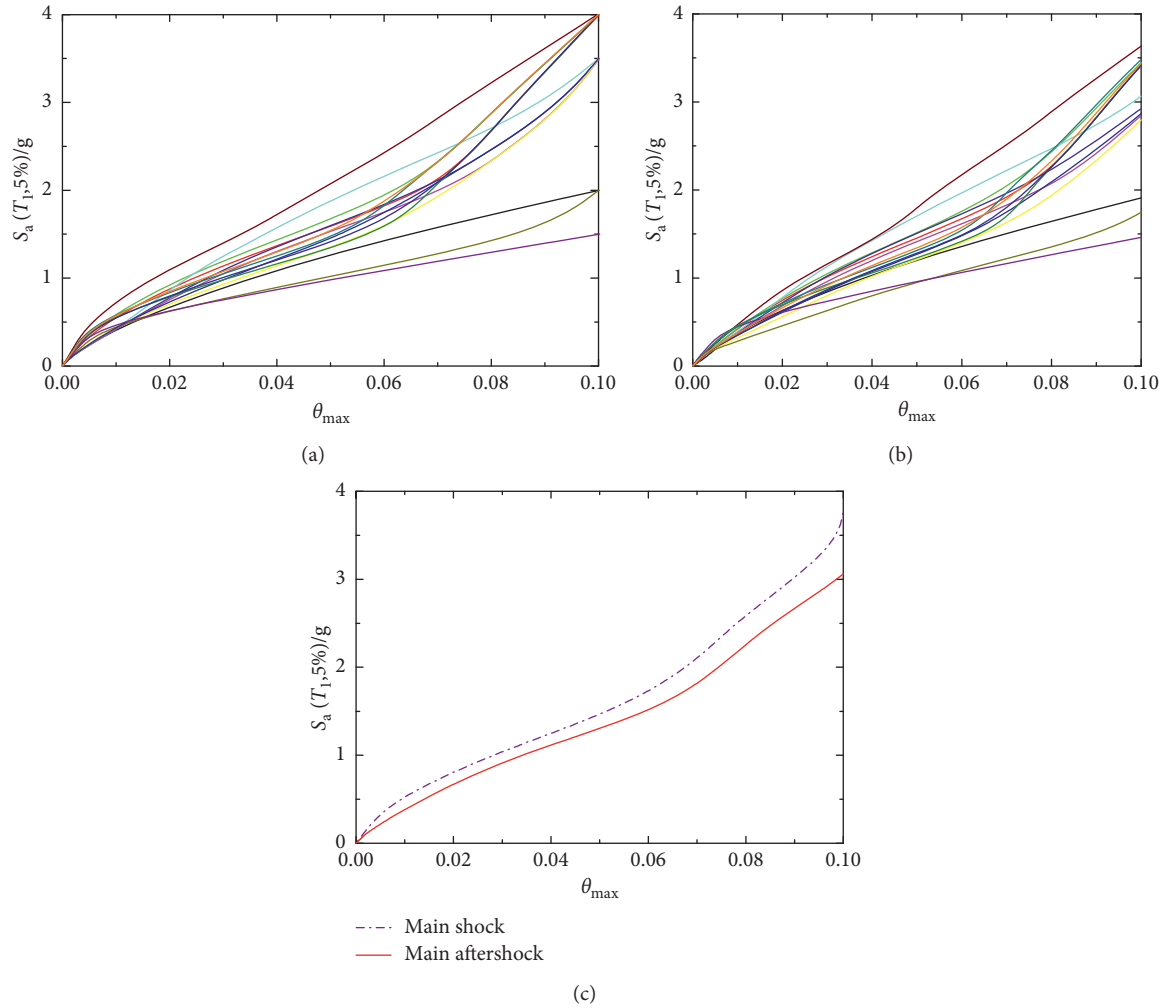

Figure 12: IDA curves. (a) The main shock ground motion. (b) The main aftershock sequence ground motion. (c) The median curve.

displacement, maximum interlayer displacement angle, and peak acceleration of each floor. The literature [37] points out that the maximum interlayer drift is directly related to the damage degree of structural members, the deformation ability between floors, and the rotation of joints and the EDP is good when investigating the seismic performance of the whole structure. Therefore, the maximum interlayer drift θ_{max} is selected as the EDP used to analyse the seismic

behaviour and damage of the SRC frame-core tube structure when subjected to earthquake action.

4.3. IDA Result Analysis. Modal analysis on the SRC frame-core tube structure is performed to determine the direction of the first-order mode shape, and the selected single main shock and main aftershock sequence ground motion are input onto the structure in this direction. The intensity of the selected ground motions is adjusted based on the $S_a(T_1, 5\%)$, and the intensity-adjusted $S_a(T_1, 5\%)$ are 0.05 g, 0.1 g, 0.2 g, 0.5 g, 1.0 g, 1.5 g, 2.0 g, 2.5 g, 3.0 g, 3.5 g, and 4.0 g. Moreover, if θ_{max} reaches 0.10, the analysis calculation is terminated and the structure cannot continue to carry load. The IDA curves of the structure under the main shock ground motion and the main aftershock sequence ground motion are obtained, as shown in Figure 12.

As seen from Figure 12(c), for the SRC frame-core tube structure, the overall trend of the IDA curves is roughly the same whether under the action of the main shock or the main aftershock. However, the θ_{max} of the structure under the action of the main aftershock is greater than under the single main shock, indicating that the seismic response of the structure increases with the occurrence of aftershocks. It can be seen from Figures 12(a) and 12(b) that when the input ground motion intensity is $S_a(T_1, 5\%) < 0.2$ g, θ_{max} increases linearly with increasing input ground motion intensity. When the input ground motion intensity is $0.2\,\text{g} < S_a(T_1, 5\%) < 2.0$ g, as the input ground motion intensity increases, the growth rate of θ_{max} begins to slow down until the input ground motion intensity $S_a(T_1, 5\%) > 2.0$ g. As the input ground motion intensity increases, the growth rate of θ_{max} starts to accelerate under some ground motions. This phenomenon is called stress hardening. Some scholars have also found similar phenomena in the simple bilinear elastoplastic system IDA, so this phenomenon is not unique to the SRC framework-core tube structure.

The structural requirements of 15 single main shocks and 15 main aftershocks under the action of an input seismic intensity $S_a(T_1, 5\%)$ are statistically processed, and the data points of θ_{max} for the same ground motion are grouped together; this assumes that the group obeys a lognormal distribution. Table 5 shows the log-mean and log-standard deviations of the structure θ_{max} subjected to various seismic intensities $S_a(T_1, 5\%)$.

5. Structural Damage Assessment Based on Seismic Vulnerability Analysis

5.1. Introduction to Seismic Vulnerability Analysis. Seismic vulnerability refers to the extent of damage caused by earthquakes in a certain area. The research object may be a single structure or a type of structure or it may be a certain area. Structural vulnerability refers to the probability that a structure will have different damage degrees under various seismic intensities or probability of exceeding a certain limit state. The mathematical expression for structural seismic vulnerability is

$$F_R(i) = P(LS \mid IM = i) = \int_y^{\infty} f_{R|I}[r \mid i]\,dr, \tag{2}$$

where F_R is the seismic vulnerability; $P[\cdot]$ is the exceeding probability; and IM is the index of ground motion intensity. In this paper, $S_a(T_1, 5\%)$ is selected as the input ground motion intensity index; $f_{R|I}[r|i]$ is a probability density function (PDF) for structural requirements of the ground motion intensity measure $IM = i$.

It is assumed that the structural engineering demand parameter EDP and the ground motion intensity measure IM satisfy the exponential function relationship of the following equation:

$$EDP = \alpha(IM)^{\beta}. \tag{3}$$

The logarithm is taken of the formula above, and the engineering demand parameter θ_{max} and ground motion intensity index $S_a(T_1, 5\%)$ selected in this paper are substituted, and the following formula is obtained:

$$\ln(\theta_{max}) = a + b\ln(S_a(T_1, 5\%)), \tag{4}$$

where a and b are constants, and $a = \ln\alpha$, $b = \beta$, the value of which can be obtained by linear regression analysis of IDA calculation results for multiple ground motions.

It is assumed that the seismic demand probability function D and the structural capability parameter probability function C satisfy a normal distribution after taking the logarithm. The vulnerability curve of the structure indicates the conditional probability that the structural demand D exceeds the structural capability parameter C under various seismic intensities, named the exceeding probability P_f of the structure:

$$P_f = P(C \mid D < 1), \tag{5}$$

Let $Z = C - D$, assuming that C and D are independent random variables, therefore, Z also obeys a normal distribution, and equation (5) can be expressed as

$$P_f = \left[\frac{\ln\mu_d - \ln\mu_c}{\sqrt{\beta_c^2 + \beta_d^2}}\right], \tag{6}$$

where μ_c and β_c are the mean and standard deviation of the structure seismic capacity, respectively; μ_d and β_d are the mean and standard deviation of the structural requirements under earthquake, respectively; and Φ is the standard positive distribution function. Substituting equation (4) into equation (6), the P_f of the structure under ground motion is

$$P_f = \phi\left[\frac{\ln\left[\alpha(S_a(T_1, 5\%))^{\beta}/\mu_c\right]}{\sqrt{\beta_c^2 + \beta_d^2}}\right], \tag{7}$$

where β_c and β_d can be determined by statistical analysis or obtained according to structural vulnerability curve parameters. FEMA350 [38] pointed out that when the vulnerability curve takes $S_a(T_1, 5\%)$ as the independent variable, the value of $\beta_c^2 + \beta_d^2$ is 0.633, and when PGA is taken as the independent variable, the value of $\beta_c^2 + \beta_d^2$ is 0.707.

Table 5: The structural requirements.

$S_a(T_1, 5\%)$	Under the main shock		Under the main aftershock	
	Log-mean of θ_{max}	Log-standard deviations of θ_{max}	Log-mean of θ_{max}	Log-standard deviations of θ_{max}
0.05	−7.334	0.147	−6.972	0.209
0.10	−6.595	0.159	−6.280	0.200
0.20	−5.838	0.253	−5.464	0.136
0.50	−4.455	0.330	−4.373	0.254
1.00	−3.565	0.294	−3.411	0.232
1.50	−2.924	0.287	−2.798	0.251
2.00	−2.656	0.213	−2.558	0.193
2.50	−2.517	0.133	−2.420	0.120
3.00	−2.421	0.090	−2.324	0.083
3.50	−2.346	0.051	−2.251	0.048
4.00	−2.301	0.002	−2.205	0.002

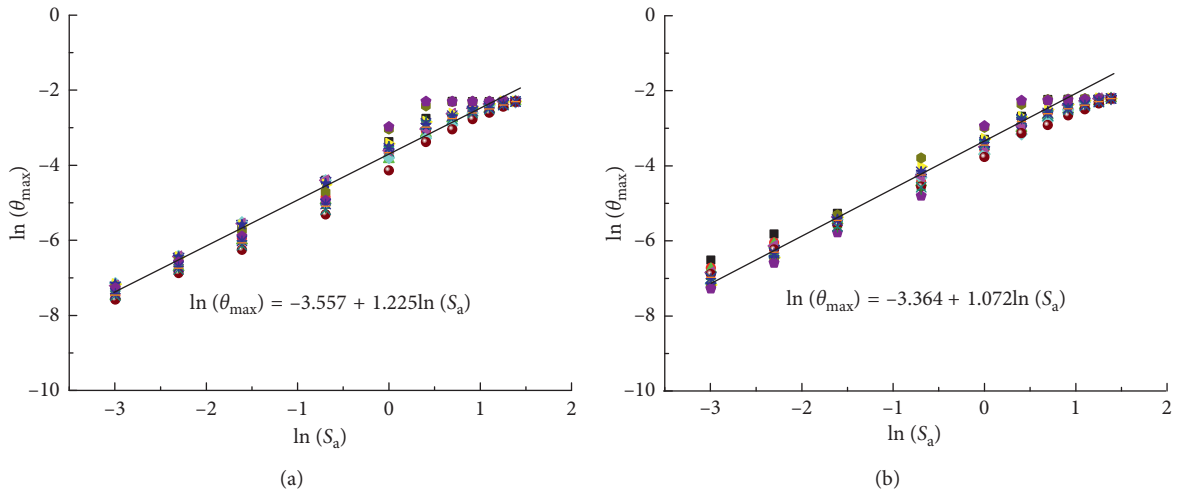

Figure 13: Linear regression analysis. (a) Main shock. (b) Main aftershock.

5.2. Determination of Probability Model Parameters. Set the logarithm of the engineering demand parameter θ_{max} and the ground motion intensity index $S_a(T_1, 5\%)$ and establish a coordinate system with $\ln(S_a(T_1, 5\%))$ as the abscissa and $\ln(\theta_{max})$ as the ordinate. The results of IDA analysis in Figure 12 are added to the coordinate system and subjected to linear regression analysis, as shown in Figure 13. The linear relationship of $\ln(S_a(T_1, 5\%))$–$\ln(\theta_{max})$ under the main shock and main aftershock is obtained as follows:

$$\begin{aligned} \ln(\theta_{max}) &= -3.557 + 1.225 \ln(S_a), \text{ (main shock)}, \\ n(\theta_{max}) &= -3.367 + 1.072 \ln(S_a). \text{ (main aftershock)}. \end{aligned} \tag{8}$$

The goodness of fit R^2 values for the two linear regression analyses were 0.965 and 0.968, respectively, and their values were very close to 1.0, indicating that the $\ln(S_a(T_1, 5\%))$ and $\ln(\theta_{max})$ scatter values are linearly correlated. The parameters α and β can be obtained by using equation (4). For a single main shock case, $\ln\alpha = -3.557$, so $\alpha = 0.029$ and $\beta = b = 1.225$; for the main aftershock condition, $\ln\alpha = -3.364$, so $\alpha = 0.035$ and $\beta = b = 1.072$.

5.3. Structural Performance Level Division and Determination of Quantitative Index Limits. The division of structural performance level directly affects the accuracy of structural seismic performance evaluation and the trend of the seismic vulnerability curve. The definition of structural performance level is essentially a definition of the expected and limited ultimate failure states. At present, the division of performance level has not reached a unified opinion. The FEMA350 [38] divides the structural performance levels into operational performance (OP), immediate occupancy (IO), life safety (LS), and collapse prevention (CP), and the expected seismic performance situation of the structure under various performance levels is defined. In the literature [39], the seismic performance levels of super-high-rise hybrid structures are divided into four levels: complete workability, basic workability, workability after repair, and life safety. However, at present, there are relatively few studies on the performance level division of the SRC framework-core tube structure. The limit state and the performance levels of the SRC framework-core tube structure proposed by Zhang [36] are adopted in this paper, as shown in Table 6.

Table 6: Limit states and its corresponding description of the performance state.

Limit states	Performance level	Description of performance state
LS_1	Complete workability	The structure is intact, the stressed members are almost undamaged, and the building can still work safely.
LS_2	Basic workability	The structure is basically intact, and the main load-carrying members are slightly damaged. Slight vertical cracks begin to occur in the coupling beam, and small oblique cracks may appear in walls. The whole structure is in an elastic state with no yielding and can continue to be used after simple repair.
LS_3	Workability after repair	The structure is greatly damaged, both structural and nonstructural members are damaged, and vertical cracks in the coupling beam and oblique cracks in the wall are developed. The structural members have large residual deformation and need to be repaired.
LS_4	Life safety	Structures and members are severely damaged, cracks in beams and walls extend to a large extent, and the yielding status of the coupling beam and walls is obtained. The lateral deformation of the lateral load resistance components is observed obviously, and the structure is in a plastic working status.

Table 7: Damage states and quantitative index.

Damage states	Basically intact	Slight damage	Moderate damage	Severe damage	Collapse
Quantitative index	$\leq LS_1$	LS_1~LS_2	LS_2~LS_3	LS_3~LS_4	$\geq LS_4$

Table 8: Interlayer drift limits of the frame-core tube structure and the hybrid structure.

Structural height	Limit states			
	LS_1	LS_2	LS_3	LS_4
≤150 m	1/800	1/400	1/200	1/100
≥250 m	1/500	1/250	1/150	1/100

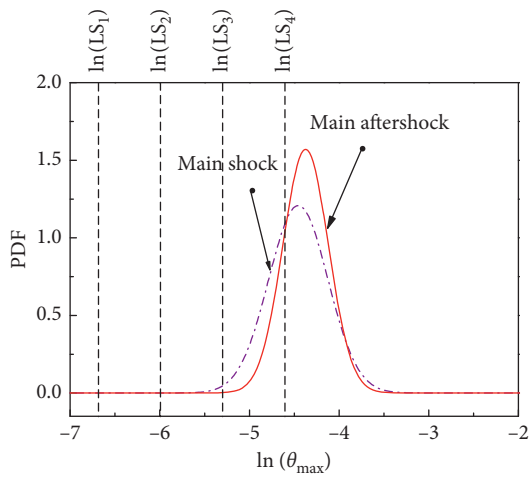

Figure 14: PDF of structural requirements ($S_a(T_1, 5\%) = 0.5$ g).

Referring to the Chinese seismic intensity scale [30], this paper divides the failure state of SRC frame-core tube structures into five grades: basically intact, slight damage, medium damage, severe damage, and collapse. Table 7 shows the correspondence between the performance level quantitative indicators and the various damage states.

In this paper, the maximum interlayer drift θ_{max} is selected as the quantitative limit index of performance level. The interlayer drift limits of the frame-core tube structure and the hybrid structure shown in Table 8, which are specified in the literature [39], are taken as the quantified index limits for the following structural analysis.

5.4. Seismic Vulnerability Analysis. Table 5 shows the log-mean and log-standard deviation of the maximum structure interlayer drift θ_{max} under various ground motion main shocks and main aftershocks. Combined with the quantitative index limits for each performance level, the probability density function curve for structural requirements under various seismic intensities can be obtained. Taking $S_a(T_1, 5\%) = 0.5$ g as an example, the probability density function curve of the structural requirements under the action of the main shock and the main aftershock is shown in Figure 14. The four vertical lines from left to right in the figure represent the logarithm of the quantified index limits corresponding to the performance level of the complete workability, basic workability, workability after repair, and life safety. It is easy to find from the figure that the four vertical lines divide the probability density function into five regions, namely, basically intact, slight damage, moderate damage, severe damage, and collapse states. Under the ground motion intensity of $S_a(T_1, 5\%) = 0.5$ g, the mean value of θ_{max} under the main aftershock sequence ground motion is greater than under the single main shock. The probability of the structure being in various damage states is shown in Table 9. The structure collapse probability under the action of a single main shock is 59.88%, and under the action of the main aftershock, it is 73.44%, which is increased by 13.56%. In addition, the proceeding probability of various structural performance levels under different seismic intensities can be obtained by equation (7). The values are shown in Table 10.

Based on the data in Table 10, the spline curve is used for interpolation, and finally the relationship between the proceeding probability P_f and the intensity index $S_a(T_1, 5\%)$ under the action of the main shock and the main aftershock is obtained, which is the seismic vulnerability curve. The seismic

Table 9: Probability of the structure being in various damage states (%).

Ground motions	Damage state				
	Basically intact	Slight damage	Moderate damage	Severe damage	Collapse
Main shock	0.21	2.11	10.79	27.02	59.88
Main aftershock	0.06	0.83	5.82	19.85	73.44

Table 10: Probability of exceeding a structural performance level under various seismic intensities.

$S_a(T_1, 5\%)$ (g)	Structural performance level							
	LS_1		LS_2		LS_3		LS_4	
	Main shock	Main aftershock	Main shock	Main aftershock	Main shock	Main aftershock	Main shock	Main aftershock
0.05	24.78	55.46	6.03	23.15	0.77	5.42	0.05	0.66
0.10	65.02	85.80	31.37	57.92	8.75	25.10	1.29	6.15
0.20	92.69	97.75	71.97	87.16	38.61	60.36	12.29	27.14
0.50	99.79	99.94	97.68	99.11	86.89	93.28	59.88	73.44
1.00	100.00	100.00	99.89	99.95	98.57	99.25	90.62	94.06
1.50	100.00	100.00	99.99	99.99	99.75	99.85	97.39	98.24
2.00	100.00	100.00	100.00	100.00	99.94	99.96	99.15	99.37
2.50	100.00	100.00	100.00	100.00	99.98	99.99	99.68	99.74
3.00	100.00	100.00	100.00	100.00	99.99	100.00	99.87	99.88
3.50	100.00	100.00	100.00	100.00	100.00	100.00	99.94	99.94
4.00	100.00	100.00	100.00	100.00	100.00	100.00	99.97	99.97

vulnerability curve of each performance level under the action of a single main shock and the main aftershock is shown in Figure 15. It can be seen that the proceeding probability of each performance level increases with increasing seismic intensity. Furthermore, when the input ground motion intensity is less than a certain critical value, the proceeding probability of the structure under main aftershock is always larger than those subjected to the single main shock. When the input ground motion intensity reaches a certain threshold, the proceeding probability of the two cases is not much different. The reason is that when the proceeding probability of the structure under a single main shock is already large, the aftershock has little contribution. It can be seen that the more unfavourable the performance level, the larger the critical value of ground motion intensity. The critical values corresponding to the four performance levels of complete workability, basic workability, workability after repair, and life safety are 0.8 g, 1.1 g, 1.5 g, and 2.0 g, respectively.

5.5. Comparative Analysis of Earthquake Vulnerability Matrix. The seismic impact coefficient α curve corresponding to intensity 8 frequent, fortification, and rare earthquakes can be determined by the Chinese seismic code [29], as shown in Figure 16. The intensity 8 earthquakes in the paper refers to the earthquakes caused the building damage of intensity 8 in the Chinese scale. According to the modal analysis, the natural vibration period of the SRC frame-core tube structure is 1.41 s. Therefore, the seismic impact coefficients of frequent, fortification, and rare earthquakes are 0.05, 0.14, and 0.29, respectively. Table 11 shows the proceeding probability of the four structural performance levels under the action of a single main shock and the main aftershock ground motion corresponding to frequent, fortification, and rare earthquakes. It can be seen that under the same fortification and performance levels, the occurrence of aftershocks will increase the proceeding probability of the SRC frame-core tube structure.

The proceeding probability can be further transformed into a seismic vulnerability matrix. Taking the main aftershock sequence ground motion as an example, when the structure is subjected to an intensity 8 rare earthquake, the probability that the structure is in a basically intact state is 100–97.78% = 2.22%; the probability of being in a slight damage state is 100%−2.22%−88.83% = 8.95%; the probability of being in moderate damage state is 100%−2.22%−8.95%−68.27% = 20.56%; the probability of being in severe damage state is 100%−2.22%−8.95%−20.56%−40.33% = 27.94%. The probability of being in a collapse state is 100%−2.22%−8.95%−20.56%−27.94% = 40.33%. By analogy, the probability that the structure is in various damage states in other cases can be calculated. The results are shown in Table 12. It can be seen that under the action of the main aftershock sequence, when an intensity 8 frequent earthquake is encountered, the probability of the structure being in a basically intact state is 48.77%, the probability of the structure being in a slight damage state is 26.21%, and the probability of being in moderate damage state is 17.24%. The probability of being in a state of severe damage is 6.37%, and the probability of being in a collapse state is 1.41%. When a fortification earthquake of intensity 8 is encountered, the probability of the structure being in basically intact, slight damage, moderate damage, severe damage, and collapse state is 10.72%, 21.19%, 29.60%, 23.86%, and 14.63%, respectively. When a rare earthquake of intensity 8 is encountered, the probability of the structure being basically intact, slightly damaged, moderately damaged, severely

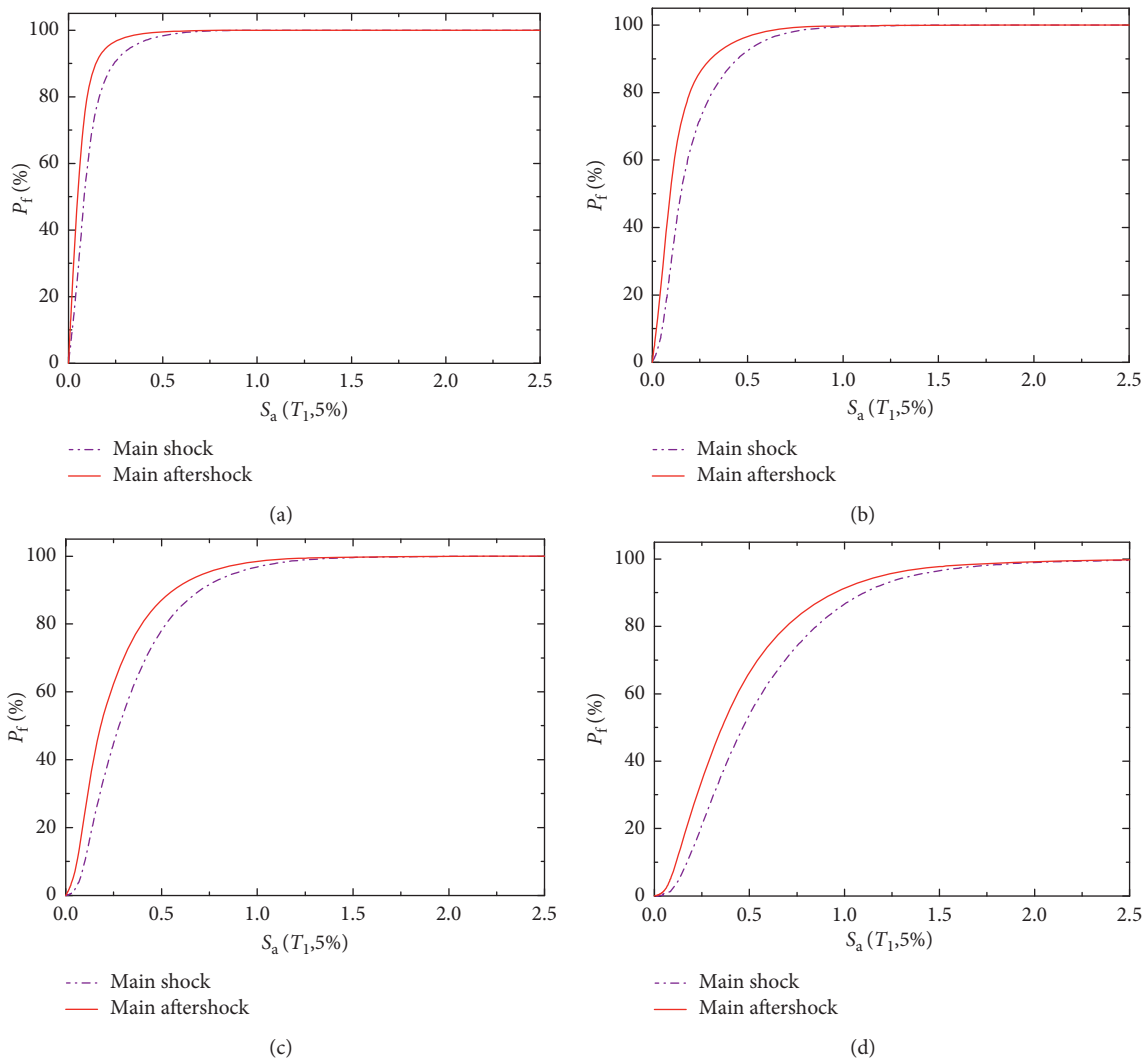

Figure 15: Vulnerability curves of various performance levels under two kinds of earthquakes. (a) LS_1. (b) LS_2. (c) LS_3. (d) LS_4.

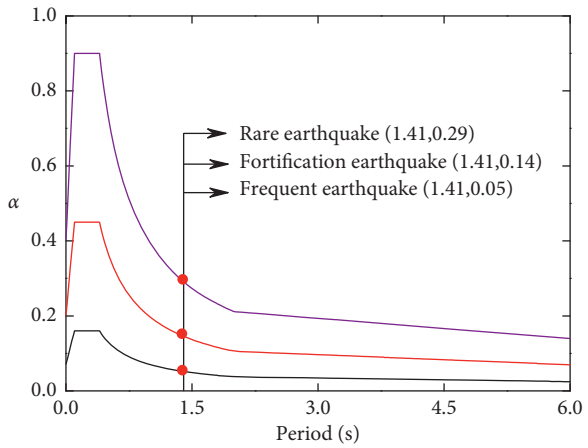

Figure 16: Spectral acceleration intensity of frequent, fortified, and rare earthquakes.

damaged, and in a collapse state is 2.22%, 8.95%, 20.56%, 27.94%, and 40.33%, respectively.

Moreover, with increasing seismic intensity input, the appearance of aftershocks causes the structure to develop to an unfavourable state of destruction. For example, when encountering an intensity 8 frequent earthquake, the probability of the structure being in slight and moderate damage states under the action of the main aftershock are 8.16% and 10.03% higher than under the main shock itself, respectively; when encountering an intensity 8 fortification earthquake, the probability of the structure being in moderate damage, severe damage, and collapse states under the action of the main aftershock is 3.66%, 9.23%, and 8.72% higher than under the main shock, respectively; when encountering an intensity 8 rare earthquake, the probability of the structure being in serious damage and collapse states under the action of the main aftershock are 2.71% and 13.63% higher than for the main shock, respectively.

Table 11: Exceeding probability of structural performance level.

Earthquake fortification level	Complete workability			Basic workability			Workability after repair			Life safety		
	Main shock	Main aftershock	D value	Main shock	Main aftershock	D value	Main shock	Main aftershock	D value	Main shock	Main aftershock	D value
Intensity 8 frequent earthquakes	27.29	51.23	23.94	9.24	25.02	15.78	2.03	7.78	5.75	0.15	1.41	1.26
Intensity 8 fortification earthquakes	74.39	89.28	14.89	46.48	68.09	21.61	20.54	38.49	17.95	5.91	14.63	8.72
Intensity 8 rare earthquakes	92.90	97.78	4.88	77.34	88.83	11.49	51.93	68.27	16.34	26.70	40.33	13.63

Table 12: Seismic vulnerability matrix of the structure under main shock and main aftershock ground motion (%).

Earthquake fortification level	Basically intact		Slight damage		Moderate damage		Severe damage		Collapse	
	Main shock	Main aftershock	Main shock	Main aftershock	Main shock	Main aftershock	Main shock	Main aftershock	Main shock	Main aftershock
Intensity 8 frequent earthquakes	72.71	48.77	18.05	26.21	7.21	17.24	1.88	6.37	0.15	1.41
Intensity 8 fortification earthquakes	25.61	10.72	27.91	21.19	25.94	29.60	14.63	23.86	5.91	14.63
Intensity 8 rare earthquakes	7.10	2.22	15.56	8.95	25.41	20.56	25.23	27.94	26.70	40.33

5.6. Structural Damage Assessment Based on Vulnerability Index. Although structure seismic vulnerability analysis reasonably assesses the degree of structural damage, its application in engineering is limited due to the following two characteristics of seismic vulnerability results: (1) the probability of the seismic vulnerability results: the seismic vulnerability curve and the vulnerability matrix all appear as a form of probability. The expression of this probability is not intuitive and is not easily accepted by engineers. (2) The multilevel of seismic vulnerability results: the seismic vulnerability curve is usually expressed as the proceeding probability of the structure at multiple performance levels. However, from the perspective of structural seismic damage assessment, engineers tend to use a single magnitude to evaluate the structure damage degree, rather than the proceeding probability of the multiple performance levels. For this problem, the vulnerability index [23] is used to assess the degree of seismic damage to the SRC framework-core tube structure. In the postearthquake survey, the seismic damage index [30] is used to evaluate the degree of structural damage, the seismic vulnerability curve is used to calculate the probability of various structural damage states, and the mathematical expectation of the seismic damage index is defined as the vulnerability index.

The damage state probability $P(\mathrm{DS_i}|S_a(T_1, 5\%)$ is defined as the difference between the proceeding probability of the adjacent structure performance level, and the calculation formula is as follows:

$$P\left(\mathrm{DS}_i \mid S_a\left(T_1, 5\%\right)\right) = \begin{cases} 1 - P\left(\mathrm{LS}_1 \mid S_a\left(T_1, 5\%\right)\right), & i = 1, \\ P\left(\mathrm{LS}_{i-1} \mid S_a\left(T_1, 5\%\right)\right) - P\left(\mathrm{LS}_i \mid S_a\left(T_1, 5\%\right)\right), & i = 2, 3, \ldots, N, \\ P\left(\mathrm{LS}_N \mid S_a\left(T_1, 5\%\right)\right), & i = N + 1. \end{cases} \tag{9}$$

where N is the number of structural performance level divisions; then, $N+1$ structural damage states can be obtained. The probability values of the various structural damage states can be obtained using the data in equation (9) and Table 9. Figure 17 shows the damage state probability curve for the SRC frame-core tube structure under the action of the main shock and the main aftershock. It can be seen that with increasing seismic intensity, the probability of the structure being in a basically intact state decreases, the probability of the structure being in a collapse state increases, and the probability of the structure being in other damage states increases first and then decreases.

The vulnerability index (VI) is calculated as

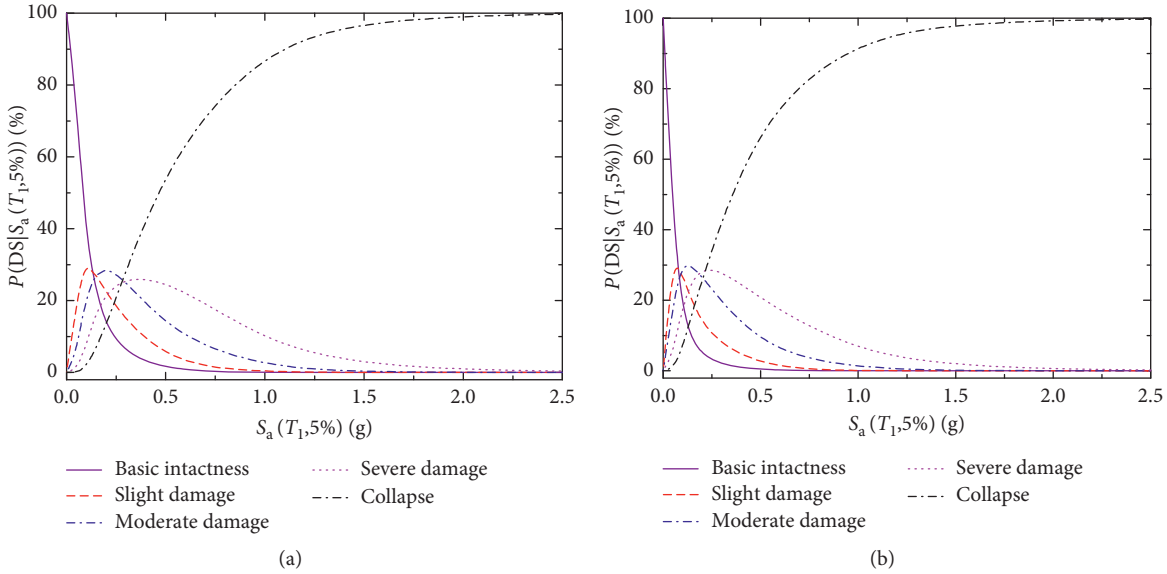

Figure 17: Probability curves of various damage states. (a) Main shock. (b) Main aftershock.

Table 13: Damage state and its corresponding damage index [30].

Damage index	Damage state				
	Basically intact	Slight damage	Moderate damage	Severe damage	Collapse
$DF_{i,U}$, $DF_{i,L}$ (%)	(0, 10]	(10, 30]	(30, 55]	(55, 85]	(85, 100]
$DF_{i,M}$ (%)	5	20	42.5	70	92.5

Table 14: Vulnerability index of the structure under the main shock/main aftershock.

$S_a(T_1, 5\%)$	Vulnerability index (%)					
	VI_L		VI_M		VI_U	
	Main shock	Main aftershock	Main shock	Main aftershock	Main shock	Main aftershock
0.00	0.00	0.00	5.00	5.00	10.00	10.00
0.05	3.89	11.73	10.29	20.17	16.70	28.60
0.10	15.35	28.28	24.51	39.19	33.66	50.09
0.20	37.00	50.44	48.48	61.98	59.96	73.52
0.50	69.20	75.17	79.32	84.47	89.43	93.77
1.00	81.80	83.02	89.97	90.95	98.13	98.87
1.50	84.15	84.43	91.84	92.06	99.53	99.69
2.00	84.73	84.80	92.29	92.35	99.85	99.89
2.50	84.90	84.92	92.42	92.44	99.95	99.96
3.00	84.96	84.96	92.47	92.47	99.98	99.98
3.50	84.98	84.98	92.49	92.49	99.99	99.99
4.00	84.99	84.99	92.49	92.49	100.00	100.00

$$VI = \sum_{i=1}^{5} \mathrm{DF} \times P\left(\mathrm{DS}_i \,\middle|\, \mathrm{S_a}\left(T_1, 5\%\right)\right), \tag{10}$$

where DF_i ($i = 1$, 2, 3, 4, and 5) stands for a seismic damage index for five damage states: the basically intact, slight damage, moderate damage, severe damage, and collapse states. $DF_{i,U}$, $DF_{i,L}$, and $DF_{i,M}$, respectively, represent the upper limit, lower limit, and mean value of the seismic damage index DF_i. The values are shown in Table 13.

Using formula (10) and the damage state probability of the structure in Figure 17, the lower limit value VI_L, mean value VI_M, and upper limit value VI_U of the structural vulnerability index for the main shock and main aftershock under various input ground motion intensities are obtained and shown in Table 14. Using the data in Table 14, the coordinate system with $S_a(T_1, 5\%)$ as the abscissa and VI as the ordinate is established, and the spline curve is used to interpolate between a limited number of discrete points. The seismic vulnerability

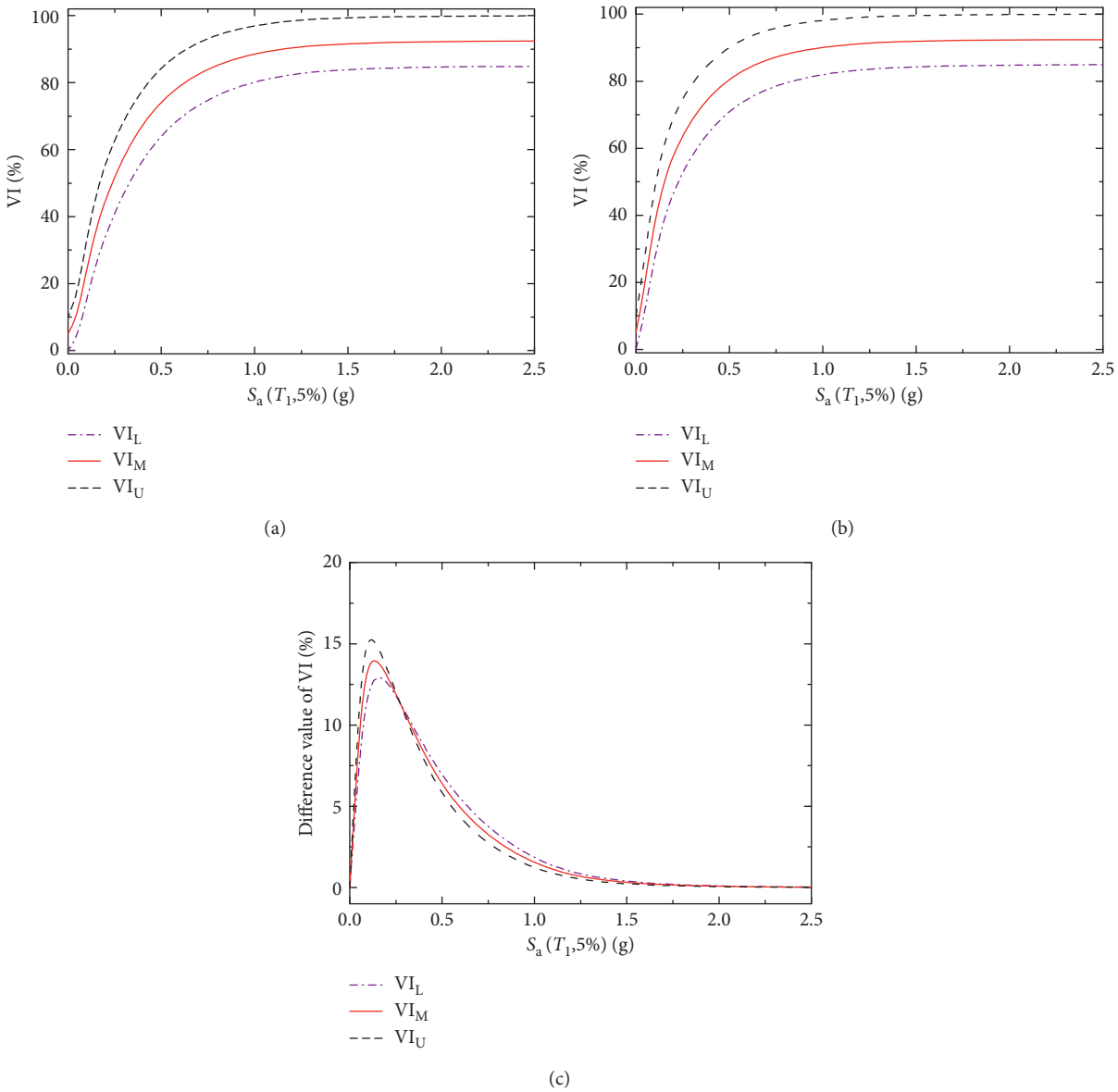

Figure 18: Vulnerability index curves. (a) Main shock. (b) Main aftershock. (c) Difference value.

Table 15: Lower limit, mean and upper limit values of the vulnerability index (%).

Ground motion	Intensity 8 frequent earthquake			Intensity 8 fortification earthquake			Intensity 8 rare earthquake		
	VI_L	VI_M	VI_M	VI_L	VI_M	VI_M	VI_L	VI_M	VI_M
Main shock	5.13	11.76	18.40	23.64	33.59	43.55	45.75	56.62	67.50
Main aftershock	12.50	20.77	29.05	36.56	47.59	54.62	56.71	67.50	78.29
Different	7.37	9.01	10.65	12.92	14.00	11.07	10.96	10.88	10.79

index curve for the structure under the action of the main aftershock and the main shock is finally drawn in Figure 18. It can be seen from Figures 18(a) and 18(b) that the structural vulnerability index of a single main shock and main aftershock increases with increasing input ground motion intensity; however, the growth rate decreases gradually. Figure 18(c) gives the curve of the structural vulnerability index difference between the two

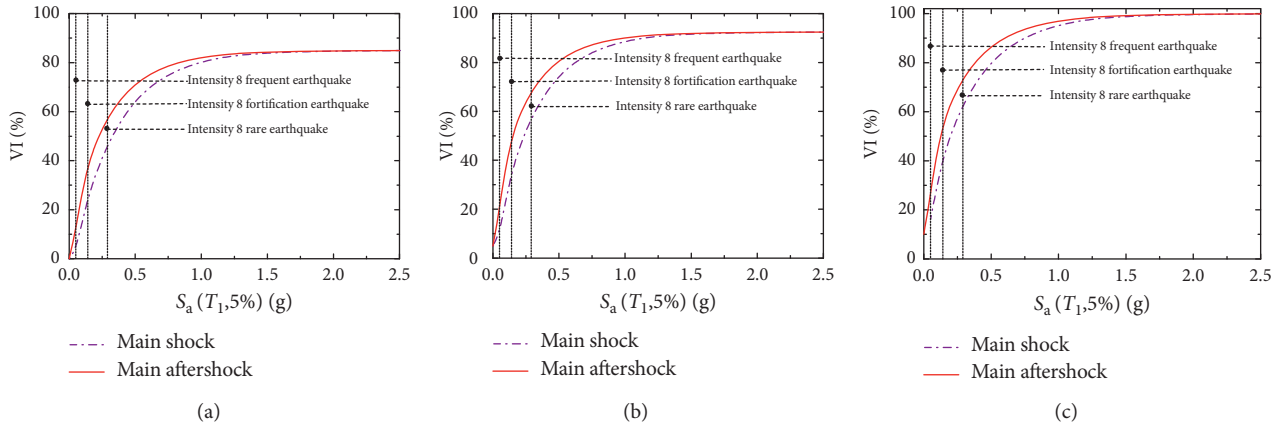

Figure 19: Vulnerability index curves. (a) Lower limit value. (b) Mean value. (c) Upper limit value.

types of ground motions. It can be seen that the difference of the structural vulnerability index increases first and then decreases with increasing seismic intensity. The variation of the lower limit, mean, and upper limit values is consistent. The ground motion intensity at the peak of the vulnerability index difference is $S_a(T_1, 5\%) = 0.15$ g.

To investigate the damage degree of the SRC frame-core tube structure under the main aftershock sequence ground motion and whether it can achieve the expected seismic fortification target, the structural vulnerability index under the action of intensity 8 frequent, fortification, and rare earthquakes can be obtained based on Formula (10) and Table 12. The values of the vulnerability index are shown in Table 15, and the curves are depicted in Figure 19. It can be seen from Figure 19 that the vulnerability index increases with increasing input ground motion intensity. When the ground motion intensity is $S_a(T_1, 5\%) < 1.5$ g, the structural vulnerability index of the main aftershock sequence ground motion is higher than the single main shock by 3~15%. When the input ground motion intensity is $S_a(T_1, 5\%) > 1.5$ g, the structural vulnerability index under a single main shock and main aftershock is basically the same. The reason is that the structure has a large degree of damage under the action of the main shock ground vibration, and the aftershocks contribute less to the structural damage.

Furthermore, combined with the damage index value in Table 13, the lower limit of the vulnerability index is used as the damage evaluation index. Under the action of a single main shock, the lower limit of the damage index obtained from the SRC frame-core tube structure when suffering an intensity 8 frequent earthquake is 5.13%, and the structure is in a basically intact state. When subjected to an intensity 8 fortification earthquake, the lower limit of the structural vulnerability index is 23.64% and the structure is in a state of slight damage. When subjected to an intensity 8 rare earthquake, the lower limit of the structural vulnerability index is 45.75% and the structure is in a moderately damaged state. Under the action of the main aftershock, when the SRC frame-core tube structure suffers intensity 8 frequent, fortification, and rare earthquakes, the lower limit of the structural vulnerability index is 12.50%, 36.56%, and 56.71%, respectively, and the structure is in a state of slight, moderate, and severe damage. The structural vulnerability index of the structure subjected to intensity 8 frequent, fortification, and rare earthquakes under the action of the main aftershock is 7.37%, 9.01%, and 10.65% larger, respectively, than under the single main shock. Similarly, when the upper limit of the vulnerability index is used as the damage evaluation index, the structural vulnerability index of a structure subjected to intensity 8 frequent, fortification, and rare earthquakes under the action of the main aftershock is 12.92%, 14.00%, and 11.07% larger, respectively, than under the single main shock. When the mean value of the vulnerability index is used as the damage evaluation index limit, the structural vulnerability index of the structure subjected to intensity 8 frequent, fortification, and rare earthquakes under the action of the main aftershock is 10.96%, 10.88% and 10.79%, respectively, larger than under the single main shock.

The vulnerability index of the structure subjected to an intensity 8 earthquake under the main aftershock is approximately 10% larger than under the single main shock. When considering the influence of the series aftershocks after the main aftershocks, the SRC frame-core tube structure is in a state of severe damage under a rare earthquake, but it does not collapse. The structure is in a moderate damage state under the action of a fortification earthquake, whereas it is in a state of slight damage under the action of a frequent earthquake. Therefore, the SRC frame-core tube structure designed according to the current Chinese specifications can also achieve the requirements as follows: facing small earthquakes, the structure is not damaged, facing medium earthquakes, the structure can be repaired, and facing strong earthquakes, the structure does not fall, under the action of the main aftershock sequence ground motion.

6. Conclusions

Based on the IDA method, the vulnerability of a typical 20-storey SRC frame-core tube structure is analysed using Perform-3D, a nonlinear analysis software. The vulnerability matrix is calculated, and the failure state probability of the

structure under various earthquake intensities is investigated. The damage degree of the SRC frame-core tube structure under the action of the main aftershock sequence and the main shock ground motion is analysed by VI. The following conclusions can be drawn.

There is a critical value of ground motion intensity for each performance level. The critical values corresponding to the performance levels of complete workability, basic workability, workability after repair, and life safety are 0.8 g, 1.1 g, 1.5 g, and 2.0 g, respectively. The seismic vulnerability matrix shows that aftershocks make the structure develop a more disadvantageous failure state.

When the ground motion intensity is $S_a(T_1, 5\%) < 1.5$ g, the structural vulnerability index of the main aftershock sequence ground motion is higher than the single main shock by 3~15%. When the input ground motion intensity is $S_a(T_1, 5\%) > 1.5$ g, the structural vulnerability index under a single main shock and main aftershock is basically the same.

Taking the vulnerability index as an evaluation parameter, the structural vulnerability index of a structure subjected to an intensity 8 earthquake under the action of the main aftershock is approximately 10% larger than under the action of a single main shock. Meanwhile, the SRC frame-core structure designed according to the current Chinese specifications meets the expected seismic fortification target even under the main aftershock sequence ground motion.

Data Availability

The data used to support the findings of this study are available from the corresponding author upon request.

Conflicts of Interest

The authors declare that there are no conflicts of interest regarding the publication of this paper.

Acknowledgments

This work was supported by the National Key Research and Development Program (Grant no. 2017YFC0703406), the National Natural Sciences Foundation of China (Grant nos. 51608434 and 51878540), the Independent Research and Development project of State Key Laboratory of Green Building in Western China (Grant no. LSZZ202018), and the Natural Science Foundation of Shaanxi Province (Grant no. 2018JQ5167).

References

[1] S. A. Mahin, "Effects of duration and aftershocks on inelastic design earthquakes," in *Proceedings of the Seventh World Conference on Earthquake Engineering*, pp. 677–679, Istanbul, Turkey, September 1980.

[2] C. Amadio, M. Fragiacomo, and S. Rajgelj, "The effects of repeated earthquake ground motions on the non-linear response of SDOF systems," *Earthquake Engineering & Structural Dynamics*, vol. 32, no. 2, pp. 291–308, 2003.

[3] G. D. Hatzigeorgiou and D. E. Beskos, "Inelastic displacement ratios for SDOF structures subjected to repeated earthquakes," *Engineering Structures*, vol. 31, no. 11, pp. 2744–2755, 2009.

[4] G. D. Hatzigeorgiou, "Ductility demand spectra for multiple near- and far-fault earthquakes," *Soil Dynamics and Earthquake Engineering*, vol. 30, no. 4, pp. 170–183, 2010.

[5] G. D. Hatzigeorgiou, "Behavior factors for nonlinear structures subjected to multiple near-fault earthquakes," *Computers & Structures*, vol. 88, no. 56, pp. 309–21, 2010.

[6] C.-H. Zhai, W.-P. Wen, Z. Chen, S. Li, and L.-L. Xie, "Damage spectra for the mainshock-aftershock sequence-type ground motions," *Soil Dynamics and Earthquake Engineering*, vol. 45, pp. 1–12, 2013.

[7] C.-H. Zhai, W.-P. Wen, S. Li, Z. Chen, Z. Chang, and L.-L. Xie, "The damage investigation of inelastic SDOF structure under the mainshock-aftershock sequence-type ground motions," *Soil Dynamics and Earthquake Engineering*, vol. 59, pp. 30–41, 2014.

[8] K. Twigden, X. Li, M. Ali, C. Oyarzo-Vera, and N. Chouw, "Effect of harmonic excitation sequences on structures," in *Proceedings of New Zealand Society for Earthquake Enginering Conference*, p. 37, NZSEE, Wellington, New Zealand, March 2010.

[9] K. Goda and M. R. Salami, "Inelastic seismic demand estimation of wood-frame houses subjected to mainshock-aftershock sequences," *Bulletin of Earthquake Engineering*, vol. 12, no. 2, pp. 855–874, 2014.

[10] M. D. Ludovico, M. Polese, M. G. d'Aragon, A. Prota, and G. Manfredi, "A proposal for plastic hinges modification factors for damaged RC columns," *Engineering Structures*, vol. 51, pp. 99–112, 2013.

[11] H. Zhu, "Analysis of seismic capacity of damaged RC frame structure with infilled-wall," Master's thesis, Guangzhou University, Guangzhou, China, 2012.

[12] F. T. Hou, "Strength reduction factor based on main shock-aftershock sequence-type ground motions," Master's thesis, Harbin Institute of Technology, Harbin, China, 2013.

[13] J. Tao, "Study on incremental damage and collapse capacity on SDOF systems under mainshock-aftershock sequences," Master's thesis, Harbin Institute of Technology, Harbin, China, 2016.

[14] X. H. Yu, D. G. Lv, and H. Xiao, "Incremental damage spectra of mainshock-aftershock sequence-type ground motions," *Engineering Mechanics*, vol. 34, no. 3, pp. 47–53, 2017.

[15] H. H. M. Hwang and Y. K. Low, "Seismic reliability analysis of plane frame structures," *Probabilistic Engineering Mechanics*, vol. 4, no. 2, pp. 74–84, 1989.

[16] T. Rossetto and A. Elnashai, "A new analytical procedure for the derivation of displacement-based vulnerability curves for populations of RC structures," *Engineering Structures*, vol. 27, no. 3, pp. 397–409, 2005.

[17] Q. Li and B. R. Ellingwood, "Performance evaluation and damage assessment of steel frame buildings under main shock-aftershock earthquake sequences," *Earthquake Engineering & Structural Dynamics*, vol. 36, no. 3, pp. 405–427, 2010.

[18] H. Ryu, N. Luco, S. R. Uma, and A. B. Liel, "Developing fragilities for mainshock-damaged structures through incremental dynamic analysis," in *Proceedings of the Ninth Pacific Conference on Earthquake Engineering Building an Earthquake-Resilient Society*, NZSEE, Auckland, New Zealand, pp. 225–233, April 2011.

[19] M. Polese, M. Di Ludovico, A. Prota, and G. Manfredi, "Damage-dependent vulnerability curves for existing buildings," *Earthquake Engineering & Structural Dynamics*, vol. 42, no. 6, pp. 853–870, 2013.

[20] Y. T. Zhang, C. Ma, Z. M. Guo, X. J. Du, and C. F. Liu, "Seismic fragility analysis for RC frame structures with

various moment magnifying coefficients," *Journal of Building Structures*, vol. 35, no. 2, pp. 29–37, 2014.

[21] Y. Y. Li, "The seismic response analysis and fragility analysis of RC frame structure based on mainshock-aftershock ground motions," Master's thesis, Harbin Institute of Technology, Harbin, China, 2014.

[22] J. F. Xu, J. Chen, and G. Ding, "Fragility analysis and life cycle cost assessment of RC frame under mainshock-aftershock seismic sequences through IDA," *Earthquake Engineering and Engineering Dynamics*, vol. 35, no. 4, pp. 206–212, 2015.

[23] D. G. Lv, G. Q. Jin, and X. H. Yu, "Modified seismic fragility analysis of reinforced concrete frame structures in consideration of collapse probability," *Journal of Building Structures*, vol. 37, no. 9, pp. 26–32, 2016.

[24] X. H. Yu, D. G. Lv, and F. Fan, "Seismic damage assessment of RC frame structures based on vulnerability index," *Engineering Mechanics*, vol. 34, no. 1, pp. 69–75, 2017.

[25] X. L. Lv, N. F. Su, and Y. Zhou, "IDA-based seismic fragility analysis of a complex high-rise structure," *Journal of Earthquake Engineering and Engineering Vibration*, vol. 32, no. 5, pp. 19–25, 2012.

[26] L. X. Zhang, Z. Y. Xu, J. P. Liu, and M. Y. Zhang, "Seismic vulnerability analysis of super high-rise hybrid structures based on incremental dynamic analysis," *Journal of Building Structures*, vol. 37, no. 9, pp. 19–25, 2016.

[27] C. D. Zhou, X. L. Zeng, F. Zhao, and H. Zhou, "Seismic fragility analysis for high-rise reinforced concrete chimney," *Earthquake Engineering and Engineering Vibration*, vol. 36, no. 2, pp. 173–181, 2016.

[28] X. Y. Lv, S. Z. Liu, C. H. Li, and J. H. Xing, "Seismic fragility analysis of steel latticed roof-concrete frame structure of small and medium sized railway passenger station," *Journal of Building Structures*, vol. 37, no. s1, pp. 85–92, 2016.

[29] GB 50011, *Code for Seismic Design of Buildings*, China Architecture & Building Press, Beijing, China, 2010.

[30] GB/T 17742, *The Chinese Seismic Intensity Scale*, Standards Press of China, Beijing, China, 2008.

[31] G. L. Bai, L. S. Chu, and L. H. Zhu, "Determination of plastic hinge property for steel reinforced concrete frame in nonlinear static analysis," *Journal of Xi'an University of Architecture and Technology (Natural Science Edition)*, vol. 39, no. 6, pp. 756–761, 2007.

[32] GB 50010, *Code for Design of Concrete Structures*, China Architecture & Building Press, Beijing, China, 2011.

[33] J. B. Mander, M. J. N. Priestley, and R. Park, "Theoretical stress-strain model for confined concrete," *Journal of Structural Engineering*, vol. 114, no. 8, pp. 1804–1826, 1988.

[34] B. W. Liu, K. Xu, C. Liu, and W. Wu, *Seismic Elastic-Plastic Analysis and Performance-Based Evaluation with Perform-3D*, China Architecture & Building Press, Beijing, China, 2014.

[35] JGJ3, *Technical Specification for Concrete Structures of Tall Building*, China Architecture & Building Press, Beijing, China, 2011.

[36] T. Zhang, "Seismic fragility analysis of SRC frame-core wall structure under mainshock-aftershock sequences," Master's thesis, Xi'an University of Architecture And Technology, Xi'an, China, 2018.

[37] X. W. Liang and Y. X. Ye, *Nonlinear Analysis of Concrete Structures*, China Architecture & Building Press, Beijing, China, 2nd edition, 2015.

[38] FEMA 350, *Multi-Hazard Loss Estimation Methodology: Earthquake Model, HAZUS-MH 2.1-Technical Manual*, Department of Homeland Security, FEMA, Washington, DC, USA, 2003.

[39] X. L. Lv, *Seismic Design Guidelines for Tall Buildings beyond the Scope of Design Codes*, Tongji University Press, Shanghai, China, 2009.